

# Sparse stabilization of mean-field agent dynamics through a three-operator splitting method\*

Giacomo Albi<sup>1</sup>, Dante Kalise<sup>2</sup>, Chiara Segala<sup>3</sup> and Franco Zivcovich<sup>4</sup>

**Abstract**—We study the sparse stabilization of nonlinear multi-agent systems within a mean-field optimal control framework. The goal is to drive large populations of interacting agents toward consensus with minimal control effort. In the mean-field limit, the dynamics are described by a Vlasov-type kinetic equation, and sparsity is enforced through an  $\ell_1$ - $\ell_2$  penalization in the cost functional. The resulting non-smooth optimization problem is solved via a three-operator splitting (TOS) method that separately handles smooth, non-smooth, and constraint components through gradient, shrinkage, and projection steps. A particle-based Monte Carlo discretization with random batch interactions enables scalable computation while preserving the mean-field structure. Numerical experiments on the Cucker–Smale model demonstrate effective consensus formation with sparse, localized control actions, confirming the efficiency and robustness of the proposed approach.

## I. INTRODUCTION

This paper investigates the sparse stabilization of nonlinear, second-order multi-agent systems (MAS), where each agent is characterized by position and velocity and interacts through nonlocal communication laws encoding attraction, repulsion, and alignment. Such interactions generate emergent collective behaviors typical of self-organizing biological systems [1], [2], [3] and appear in diverse contexts, from crowd motion and social dynamics [4], [5], [6], [7] to robotic swarms and AI networks [8], [9], [10].

The collective dynamics of large systems can be described at multiple scales: microscopically by ODEs and at mesoscopic or macroscopic levels by mean-field PDEs [11], [12], [13]. Deriving higher-scale models such as mean-field or kinetic equations [14] is crucial both theoretically and computationally. Mean-field formulations consistently capture macroscopic behavior by averaging microscopic fluctuations, while reducing the computational cost of simulating high-dimensional  $N$ -agent systems [15], [16], [17].

Our main goal is to design control strategies that steer the system toward consensus, namely a collective state where all agents share a common velocity. As a prototype, we consider the controlled Cucker–Smale model [18], [19], a benchmark

for self-organization and control in collective dynamics. We seek parsimonious controls acting on few agents to minimize intervention cost. Sparsity is promoted by an  $\ell_1$ -penalty in the cost functional [20], [21], [22], [23], [24], which effectively targets the most misaligned agents [25]. Since the non-smooth  $\ell_1$  term prevents standard gradient methods, we employ a three-operator splitting (TOS) algorithm [26], [27] that alternates gradient and proximal steps over smooth, non-smooth, and constrained components. Gradients are computed via adjoint equations, while proximal maps admit closed-form shrinkage and projection operators.

To ensure scalability, we adopt a mean-field formulation leading to a Vlasov-type kinetic equation for the agent density in phase space [28], [29], [30]. This model preserves the essential microscopic structure while lowering computational cost and is discretized through a Monte Carlo particle scheme with linear complexity [31], [12]. Combining mean-field modeling with proximal splitting yields a unified, scalable framework for sparse stabilization of collective dynamics. Numerical experiments on the alignment model demonstrate consensus with minimal control effort and persistent sparsity in both time and across agents.

The paper is organized as follows: Section II introduces the mean-field optimal control formulation from microscopic to mesoscopic level; Section III details the particle discretization of the mean-field control problem; Section IV describe the TOS gradient for the mean-field sparse stabilization. Finally, Section V presents different numerical results.

## II. MEAN-FIELD APPROXIMATION OF OPTIMAL MAS CONTROL

We consider a MAS of  $N$  interacting agents with states  $(x_i(t), v_i(t)) \in \mathbb{R}^d \times \mathbb{R}^d$ , where  $d$  denotes the dimension of the physical space. The evolution of each agent is governed by the second-order dynamics

$$\begin{aligned} \dot{x}_i &= v_i, \\ \dot{v}_i &= \frac{1}{N} \sum_{j=1}^N P(\|x_i - x_j\|_2)(v_j - v_i) + u_i, \end{aligned} \quad (1)$$

for  $i = 1, \dots, N$ , with initial data  $x_i(0) = x_i^0$  and  $v_i(0) = v_i^0$ . The function  $P(\cdot)$  is a symmetric, radial communication kernel describing pairwise interactions between agents, defined as

$$P(r) = (1 + r^2)^{-\kappa}, \quad \kappa > 0. \quad (2)$$

Here, the objective is to design control laws  $u_i(t)$  that drive the system toward a state of consensus where all

\*This work has been partially supported by MUR project PRIN 2022 PNRR nr. P2022JC95T, CUP: B53D23027840001; by Swiss National Science Foundation (SNSF) through the grant number 215528; GA and CS are member of INdAM GNCS group.

<sup>1</sup>Giacomo Albi is with the Department of Computer Science, University of Verona, IT, giacomo.albi@univr.it

<sup>2</sup>Department of Mathematics, Imperial College London, UK, dkaliseb@imperial.ac.uk

<sup>3</sup>Faculty of Informatics, Università della Svizzera italiana, Lugano, CH, chiara.segala@usi.ch

<sup>4</sup>Franco Zivcovich is with Department of Computer Science, University of Verona, IT, franco.zivcovich@univr.it

agents share the same velocity  $\bar{v}(t) = (N)^{-1} \sum_{j=1}^N v_j(t)$ . The term  $u(t) = (u_1(t), \dots, u_N(t)) \in \mathbb{R}^{dN}$  denotes the collection of control inputs acting on the agents, where each  $u_i : [0, T] \rightarrow U \subset \mathbb{R}^d$  and  $U$  a compact set of admissible controls, moreover, in what follows we will require that the set of admissible control is such that

$$\mathcal{U}^N = \left\{ u(\cdot) : \frac{1}{N} \int_0^T \sum_{i=1}^N \|u_i(\tau)\|_1 d\tau \leq B \right\}, \quad (3)$$

where  $B > 0$  is a fixed budget. We assume that the control vector  $u(\cdot)$  is obtained as minimizer over  $\mathcal{U}^N$  of a cost functional  $\mathcal{J}^N(u) \equiv \mathcal{J}^N(u; x^0, v^0)$  defined by

$$\begin{aligned} \mathcal{J}^N(u) = \int_0^T \frac{1}{N} \sum_{i=1}^N & \left( \|\bar{v}(t) - v_i(t)\|_2^2 \right. \\ & \left. + \alpha \|u_i(t)\|_2^2 + \beta \|u_i(t)\|_1 \right) dt, \end{aligned} \quad (4)$$

where  $\alpha, \beta \geq 0$  are penalization parameters. The first term promotes consensus among the agents, the quadratic term penalizes the overall control energy, and the  $\ell_1$ -term introduces sparsity, ensuring that only a limited number of agents or time instants are actively controlled. This type of formulation has been widely employed in the context of sparse control of alignment dynamics [18], [32], [33].

Although the microscopic control problem (1)–(4) provides an accurate description of the dynamics, its computational cost grows rapidly with  $N$ . To overcome this limitation, a mean-field approximation can be derived by considering the limit  $N \rightarrow \infty$ . In this limit, the individual-based model is replaced by a continuous distribution of agents described by a probability density function  $f(t, x, v)$  defined over the phase space  $\mathbb{R}^{2d}$ . The corresponding empirical measure associated with the microscopic system is given by  $f^N(t, x, v) = N^{-1} \sum_{i=1}^N \delta(x - x_i(t)) \otimes \delta(v - v_i(t))$ . As  $N \rightarrow \infty$ , the empirical measure  $f^N$  converges to  $f(t, x, v) \in \mathcal{M}_1(\mathbb{R}^{2d})$ , the space of probability measures with compact support, see [34], [29]. The evolution of  $f$  is governed by a Vlasov-type equation of the form

$$\partial_t f + v \cdot \nabla_x f = -\nabla_v \cdot [f(\mathcal{P}[f] + u)], \quad (5)$$

with initial data  $f(0, x, v) = f^0(x, v)$ , and where the nonlocal alignment operator  $\mathcal{P}[f] \equiv \mathcal{P}[f](t, x, v)$  is

$$\mathcal{P}[f](t, x, v) = \int_{\mathbb{R}^{2d}} P(\|x - x_*\|_2)(v_* - v) df_*,$$

where we used the shorten notation  $df_* = f(t, x_*, v_*) dx dv$ . The control  $u = u(t, x, v)$  is a distributed control acting such that  $u : [0, T] \times \mathbb{R}^{2d} \rightarrow \mathbb{R}^d$ , and obtained by minimizing the following cost functional

$$\begin{aligned} \mathcal{J}(u) := \int_0^T \int_{\mathbb{R}^{2d}} & \left( \|m[f](t) - v\|_2^2 \right. \\ & \left. + \alpha \|u\|_2^2 + \beta \|u\|_1 \right) df dt, \end{aligned} \quad (6)$$

where

$$m[f](t) = \int_{\mathbb{R}^{2d}} v df(x, v),$$

is the mean velocity of the population, and the set of the admissible control in the mean-field limit is denoted as  $\mathcal{U}$ , where the budget constrain in (3) is replaced by

$$\int_0^T \int_{\mathbb{R}^{2d}} \|u(\tau, x, v)\|_1 df d\tau \leq B. \quad (7)$$

### III. PARTICLE-BASED SCHEME FOR MEAN-FIELD SPARSE STABILIZATION

To efficiently approximate the mean-field control dynamics (5)–(6), we develop a particle-based methods based on randomized sampling similarly to methods proposed in [15], [12], [16]. Here, we combine these strategies with optimization methods for the synthesize of the optimal control.

We account for  $N_s$  particles  $\{(x_i^0, v_i^0)\}_{i=1}^{N_s}$  sampled independently from the initial distribution  $f^0(x, v)$ . The mean-field dynamics is then approximated by a time-discrete particle system evolving according to the microscopic dynamics (1). We introduce the discrete time grid  $t^n = n\Delta t$ , with  $N_T \Delta t = T$ , and simulate the system for  $i = 1, \dots, N_s$  and  $n = 0, \dots, N_T - 1$  as

$$\begin{aligned} x_i^{n+1} &= x_i^n + \Delta t v_i^n, \\ v_i^{n+1} &= v_i^n + \Delta t u_i^n \\ &+ \frac{\Delta t}{M_s} \sum_{k=1}^{M_s} P\left(\|x_i^n - x_{j_k}^n\|_2\right) (v_{j_k}^n - v_i^n), \end{aligned} \quad (8)$$

where  $\{j_1, \dots, j_{M_s}\} \subseteq \{1, \dots, N_s\}$  is a random subsample of size  $M_s \leq N_s$  drawn at each time step to approximate the interaction operator. Notice that the interaction is computed with respect to a sampled subset of agents, this reduces the cost of each update from  $\mathcal{O}(N_s^2)$  to  $\mathcal{O}(N_s M_s)$ , making the scheme feasible for large-scale simulations.

The performance of the control strategy is assessed by discretizing the mean-field cost functional (6). The discrete counterpart reads as follows

$$\begin{aligned} \mathcal{J}_{\Delta t}^{N_s}(\mathbf{u}) := \frac{\Delta t}{N_s} \sum_{n=0}^{N_T-1} \sum_{j=1}^{N_s} & \left( \|\bar{v} - v_j^n\|_2^2 \right. \\ & \left. + \alpha \|u_j^n\|_2^2 + \beta \|u_j^n\|_1 \right), \end{aligned} \quad (9)$$

where  $\{u^n\} = (u_1^n, \dots, u_{N_s}^n) \in \mathbb{R}^{dN_s}$  acts on each interval  $[t^n, t^{n+1}]$ , and we introduce the concatenated control vector

$$\mathbf{u} := (u^0, u^1 \dots u^{N_T-1}) \in \mathbb{R}^{dN_s N_T},$$

which collects all the agents' controls over the discretized time horizon. The admissible set of control (7) in the discrete setting corresponds to

$$\tilde{\mathcal{U}} = \left\{ \mathbf{u} \in \mathbb{R}^{dN_s N_T} : \|\mathbf{u}\|_1 \leq \tilde{B} \right\}, \quad (10)$$

which is a non-empty, closed, and convex set, and where  $\tilde{B} = N_s B / \Delta t > 0$  denotes the scaled budget according to (7). The discrete optimization problem reads

$$\min_{\mathbf{u} \in \tilde{\mathcal{U}}} \mathcal{J}_{\Delta t}^{N_s}(\mathbf{u}), \quad \text{s.t. (8)}. \quad (11)$$

### A. Discrete optimality conditions

We derive from (8)–(9) the set of optimality conditions for the discrete agent system introducing a Lagrangian functional that enforces the discrete dynamics (8) as constraints. Hence, let  $p^n = (p_1^n, \dots, p_{N_s}^n)$  and  $q^n = (q_1^n, \dots, q_{N_s}^n)$  be the adjoint multipliers associated with the state variables  $x^n$  and  $v^n$ , respectively, then the adjoint dynamics reads

$$\begin{aligned} p_i^n &= p_i^{n+1} + \frac{\Delta t}{M_s} \sum_{k=1}^{M_s} P'(\|x_i^n - x_{j_k}^n\|_2) \\ &\quad \langle q_{j_k}^{n+1} - q_i^{n+1}, v_{j_k}^n - v_i^n \rangle (x_{j_k}^n - x_i^n), \\ q_i^n &= q_i^{n+1} + 2\Delta t(v_i^n - \bar{v}^n) - \Delta t p_i^{n+1} \\ &\quad + \frac{\Delta t}{M_s} \sum_{k=1}^{M_s} P(\|x_i^n - x_{j_k}^n\|_2) (q_i^{n+1} - q_{j_k}^{n+1}), \end{aligned} \quad (12)$$

with terminal conditions  $p_i^{N_T} = 0$ ,  $q_i^{N_T} = 0$ . In the unconstrained setting, the variation with respect to  $\mathbf{u}$  yields, for each  $i = 1, \dots, N_s$  and  $n = 0, \dots, N_T - 1$ , to the optimality condition

$$0 \in (2\alpha u_i^n + q_i^{n+1} + \beta \partial \|u_i^n\|_1), \quad (13)$$

where  $\partial \|\cdot\|_1$  denotes the subdifferential of the  $\ell_1$ -norm. Under the admissibility constraints  $u_i^n \in \mathcal{U}_{\text{adm}}$ , the condition is complemented by the normal cone to the admissible set.

**Remark III.1.** We remark that when  $N_s = M_s = N$  the proposed particle discretization coincides to the time-discrete formulation of the optimality system associated to the optimal control problem for the microscopic system (1)–(4), and similarly to [19], [18]. For further details about the consistency results of the discretized adjoint system and its mean-field formulation we refer to [31], [35], [36].

## IV. TOS SCHEME FOR MEAN-FIELD SPARSE CONTROL

We address the solution of the discrete optimization problem (11), which is a high-dimensional non-smooth optimization problem due to the  $\ell_1$ -term promoting sparsity in the control vector  $\mathbf{u} \in \mathbb{R}^{dN_s N_T}$  and to the presence of a non-linear interaction kernel. To efficiently handle this structure, we adopt a three-operator splitting (TOS) algorithm, which extends proximal gradient methods to combine smooth quadratic terms, the non-smooth  $\ell_1$  penalty, and possible convex constraints. The solution of the resulting optimality system (8)–(12)–(13) is then obtained through the iterative TOS procedure. The discrete optimization problem (11) can be rewritten in the equivalent TOS form

$$\min_{\mathbf{u} \in \mathbb{R}^{dN_s N_T}} \mathcal{J}_1(\mathbf{u}) + \mathcal{J}_2(\mathbf{u}) + \mathcal{J}_3(\mathbf{u}), \quad (14)$$

where the first two components correspond respectively to the smooth term

$$\mathcal{J}_1(\mathbf{u}) = \frac{\Delta t}{N_s} \sum_{n=0}^{N_T-1} \sum_{i=1}^{N_s} \left( \|\bar{v}^n - v_i^n\|_2^2 + \alpha \|u_i^n\|_2^2 \right), \quad (15)$$

and the non-smooth parts related to the  $\ell_1$  penalty and the budget constraint as follows

$$\mathcal{J}_2(\mathbf{u}) = \frac{\Delta t}{N_s} \sum_{n=0}^{N_T-1} \sum_{i=1}^{N_s} \beta \|u_i^n\|_1 = \frac{\Delta t}{N_s} \beta \|\mathbf{u}\|_1,$$

and the barrier function

$$\mathcal{J}_3(\mathbf{u}) = \delta_{\tilde{\mathcal{U}}}(\mathbf{u}) := \begin{cases} 0, & \text{if } \mathbf{u} \in \tilde{\mathcal{U}}, \\ +\infty, & \text{if } \mathbf{u} \notin \tilde{\mathcal{U}}, \end{cases}$$

where the admissible set is defined in (10). Following the approach of [27], we employ the TOS scheme as a generalization of the classical gradient method, incorporating two proximal mappings for the non-smooth part, and corresponding to the shrinkage and projection operators. Starting from an initial guess  $\mathbf{u}^{(0)} \in \mathbb{R}^{dN_s N_T}$ , the algorithm generates an iterative sequence  $\mathbf{u}^{(k)}$  via

$$\begin{aligned} \mathbf{u}_{\mathcal{J}_3}^{(k)} &= \text{prox}_{\lambda \mathcal{J}_3}(\mathbf{u}^{(k)}), \\ \mathbf{u}_{\mathcal{J}_2}^{(k)} &= \text{prox}_{\lambda \mathcal{J}_2} \left( 2\mathbf{u}_{\mathcal{J}_3}^{(k)} - \mathbf{u}^{(k)} \right. \\ &\quad \left. - \lambda \nabla \mathcal{J}_1(\mathbf{u}_{\mathcal{J}_3}^{(k)}) \right), \\ \mathbf{u}^{(k+1)} &= \mathbf{u}^{(k)} + \lambda_k \left( \mathbf{u}_{\mathcal{J}_2}^{(k)} - \mathbf{u}_{\mathcal{J}_3}^{(k)} \right). \end{aligned} \quad (16)$$

Since  $\mathcal{J}_1$  depends on both  $\mathbf{u}$  and the velocity variables  $\mathbf{v}$  through the discrete dynamics (8), its gradient with respect to  $\mathbf{u}$  must account for this coupling. Using the adjoint variables  $q_i^{n+1}$  to represent this dependence, the gradient is

$$\nabla \mathcal{J}_1(u_i^n) = \frac{\Delta t}{N_s} (2\alpha u_i^n + q_i^{n+1}), \quad (17)$$

which gives the discrete-time optimality condition as the smooth component of (13). The parameter  $\lambda \in (0, 2\vartheta)$  now plays the role of the stepsize for the forward (gradient) step, consistent with the notation in [27], where  $\vartheta > 0$  denotes the cocoercivity constant of  $\nabla \mathcal{J}_1$ , inversely related to its Lipschitz constant. The relaxation parameter  $\lambda_k \in (0, (4\vartheta - \lambda)/(2\vartheta))$  controls the averaging between successive iterates.

We introduced in (16) the proximal operator, i.e. for a given convex, lower semi-continuous function  $\varphi$  defined as

$$\text{prox}_{\lambda \varphi}(w) = \arg \min_z \left\{ \frac{1}{2} \|z - w\|_2^2 + \lambda \varphi(z) \right\}.$$

To explicitly compute the first and second step of (16) we can rely on the following proposition

**Proposition IV.1.** *The proximal operators of  $\lambda \mathcal{J}_2$  and  $\lambda \mathcal{J}_3$  in (16) are given respectively by*

$$\text{prox}_{\lambda \mathcal{J}_2}(w) = \mathbb{S}_{\beta \lambda \frac{\Delta t}{N_s}}(w) \quad (18)$$

$$\text{prox}_{\lambda \mathcal{J}_3}(w) = \mathbb{P}_{\tilde{\mathcal{U}}}(w), \quad (19)$$

where the soft-thresholding operator is defined as

$$\mathbb{S}_h(w) := \text{sign}(w) [|w| - h]_+,$$

---

**Algorithm 1** TOS reduced gradient
 

---

- 1: **Input:** Inital density  $f^0(x, v)$  and final time  $T > 0$ , time step  $\Delta t > 0$ , number of time steps  $N_T$ , number of sampled agents  $N_s \geq M_s$ , parameters  $\alpha, \beta > 0$  (see (9)), tolerance  $tol > 0$ , maximum iterations  $k_{\max}$ , and initial guess  $\mathbf{u}^{(0)}$ .
  - 2: Sample initial states  $\{(x_i^0, v_i^0)\}_{i=1}^{N_s}$  from  $f^0(x, v)$ .
  - 3: Set iteration counter  $k = 0$ .
  - 4: **while**  $\|\nabla \mathcal{J}(\mathbf{u}^{(k)})\|_2 > tol$  **and**  $k < k_{\max}$  **do**
  - 5:   (i) Compute  $(\mathbf{x}^{(k)}, \mathbf{v}^{(k)})$  via (8).
  - 6:   (ii) Compute  $(\mathbf{p}^{(k)}, \mathbf{q}^{(k)})$  via (12).
  - 7:   (iii) Set step parameters  $\lambda, \lambda_k > 0$ .
  - 8:   (iv) Projection step  $\mathbf{u}_{\mathcal{J}_3}^{(k)}$  via (19).
  - 9:   (v) Evaluate gradient  $\nabla \mathcal{J}_1(\mathbf{u}_{\mathcal{J}_3}^{(k)})$  as in (17).
  - 10:   (vi) Compute auxiliary variable:
 
$$\mathbf{w}^{(k)} = 2\mathbf{u}_{\mathcal{J}_3}^{(k)} - \mathbf{u}^{(k)} - \lambda \nabla \mathcal{J}_1(\mathbf{u}_{\mathcal{J}_3}^{(k)}).$$
  - 11:   (vii) Shrinkage step  $\mathbf{u}_{\mathcal{J}_2}^{(k)} = \text{prox}_{\lambda \mathcal{J}_2}(\mathbf{w}^{(k)})$  via (18).
  - 12:   (viii) Update control:
 
$$\mathbf{u}^{(k+1)} = \mathbf{u}^{(k)} + \lambda_k (\mathbf{u}_{\mathcal{J}_2}^{(k)} - \mathbf{u}_{\mathcal{J}_3}^{(k)}).$$
  - 13:   (ix) Increment  $k \leftarrow k + 1$ .
  - 14: **end while**
- 

with  $[\cdot]_+$  the positive part applied componentwise, and the projection map is

$$\mathbb{P}_{\tilde{\mathcal{U}}}(w) := \begin{cases} w, & \text{if } \|w\|_1 \leq \tilde{B}, \\ \mathbb{S}_{\lambda^*}(w), & \text{if } \|w\|_1 > \tilde{B}, \end{cases}$$

with  $\lambda^* > 0$  chosen such that  $\|\mathbb{S}_{\lambda^*}(w)\|_1 = \tilde{B}$ .

These results follow from standard proximal operator derivations; see [26, Ch. 6, Sec. 6.2–6.4] for details.

**Remark IV.2.** The successive proximal steps in (16) ensure stability and convergence. The soft-thresholding operator  $\mathbb{S}(\cdot)$  performs the ISTA-type shrinkage that promotes sparsity, while the projection  $\mathbb{P}(\cdot)$  enforces feasibility by constraining the control to  $\tilde{\mathcal{U}}$ .

## V. NUMERICAL EXPERIMENTS

We test the performance of the sparse control strategies at both microscopic and mean-field scales.

### A. Test 1: Microscopic dynamics

We first assess the methodology on the microscopic dynamics (1), as justified by Remark III.1. We consider the one-dimensional system of  $N = 20$  agents with Cucker-Smale dynamics (1) with  $\kappa = 1$  in (2). The final horizon is set  $T = 15$  with time discretization step  $\Delta t = 0.2$ . Initial states are sampled as  $x_i^0 \sim \mathcal{N}(\mu_x^{(i)}, \sigma_x^2)$ ,  $v_i^0 \sim \mathcal{N}(\mu_v^{(i)}, \sigma_v^2)$ , where  $(\mu_x^{(1)}, \mu_v^{(1)}) = (0, -2)$ ,  $(\mu_x^{(2)}, \mu_v^{(2)}) = (0, 0)$ ,  $(\mu_x^{(3)}, \mu_v^{(3)}) = (-2, 2)$ , with  $\sigma_x = 0.2$ ,  $\sigma_v = 0.4$ , forming three clusters

that prevent consensus without control [1]. We consider the control functional (4) with a fixed budget as in (10), setting  $\tilde{B} = 120$  and  $\alpha = 0.01$  for the  $\ell_2$  regularization term, while varying  $\beta$  to induce sparsity through the  $\ell_1$  penalty. The sparse control problem is solved using the TOS scheme (16) with the following fixed parameters:  $tol = 10^{-8}$ ,  $k_{\max} = 5 \times 10^2$ ,  $\lambda = 0.1$ ,  $\lambda_k = 1$ , and  $\mathbf{u}^{(0)} = 0$ . We test  $\beta \in \{5 \times 10^{-2}, 10^{-1}, 1\}$  to study the effect of sparsity.

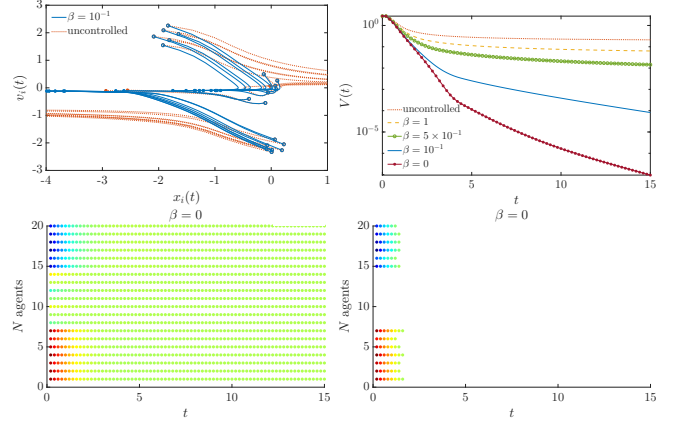


Fig. 1. **Test 1.** *Top row:* (left) uncontrolled vs. controlled trajectories for  $\alpha = 10^{-2}$ ,  $\beta = 10^{-1}$ ; (right) decay of the Lyapunov functional  $V(t) = (2N)^{-2} \sum_{i,j} |v_i(t) - v_j(t)|^2$  for different  $\beta$ . *Bottom row:* (left) active control components for  $\beta = 0$  and (right) for  $\beta = 10^{-1}$ .

Figure 1 compares uncontrolled, sparse controlled, and optimally controlled dynamics. For  $\beta = 10^{-1}$ , agents reach consensus while the uncontrolled system remains dispersed. Smaller  $\beta$  values accelerate convergence with more active controls, whereas larger  $\beta$  increase sparsity but slow alignment, showing a trade-off between efficiency and parsimony.

### B. Test 2: Mean-field sparse stabilization

We next evaluate the sparse control strategy on the mean-field Cucker–Smale model (5). The initial density  $f^0(x, v)$  reproduces the microscopic configuration of Test 1, consisting of three clusters in phase space centered at  $(\mu_x^{(i)}, \mu_v^{(i)})$  with spreads  $\sigma_x = 0.2$  and  $\sigma_v = 0.4$ . The system is initialized with  $N_s = 4 \times 10^4$  particles and simulated up to  $T = 15$  using a time step  $\Delta t = 0.2$ . The dynamics are approximated through the Monte Carlo particle scheme described in Section III with  $M_s = 100$  random batches. The mean-field cost functional (6) adopts the same regularization weight  $\alpha = 0.01$  as in Test 1, while varying the sparsity parameter  $\beta$  to assess the influence of the  $\ell_1$  penalization. The TOS algorithm is applied with the same numerical settings and stopping criteria used in the microscopic case.

Figure 2 shows the mean-field evolution in the uncontrolled case, where agents remain dispersed in both space and velocity. Figure 3 reports in the top row the sparse control case where the velocity marginal concentrates, and the spatial distribution is confined. The control efficiently promotes consensus while maintaining sparsity, as depicted in the bottom row for space (left) and velocity (right).

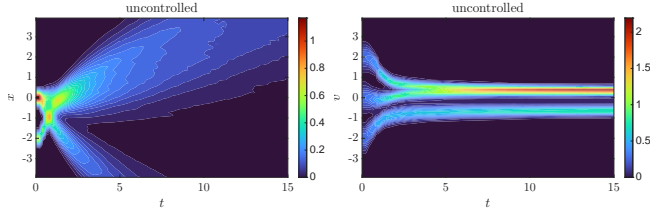


Fig. 2. **Test 2 (uncontrolled)**. Mean-field dynamics without control: left panel shows the spatial distribution, and right panel the velocity marginal.

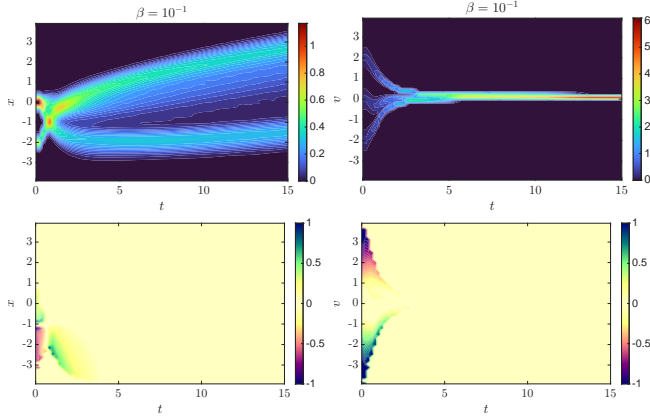


Fig. 3. **Test 2 (controlled)**. *Top row*: Mean-field dynamics with control parameters  $\alpha = 10^{-2}$ ,  $\beta = 10^{-1}$ : spatial concentration (left) and velocity alignment (right) are achieved. *Bottom row*: time evolution of control marginals in  $x$  (left) and  $v$  (right), showing strong activity initially that vanishes as consensus emerges.

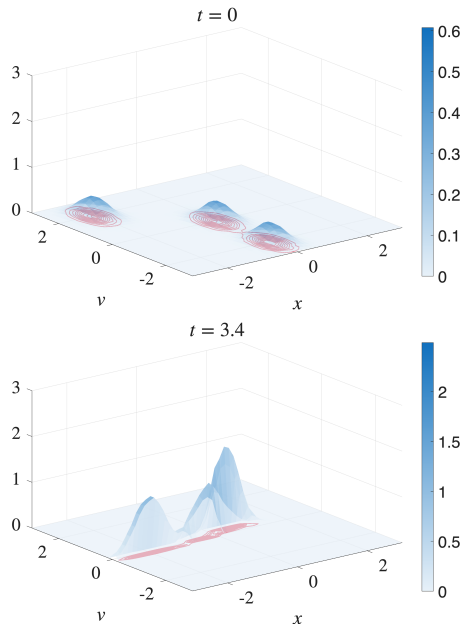


Fig. 4. **Test 2**. *Top row*: Initial configuration at  $t = 0$ ; *Bottom row*: controlled state at  $t = 3.4$  for  $\beta = 10^{-1}$ .

Figure 4 illustrates the phase-space evolution of the mean-field density. Initially, agents form three clusters that merge into a single aligned group, where here we depict the behavior at time  $t = 3.4$  where alignment is already almost reached. Finally, the control performance is assessed using the Lyapunov functional  $V(t) = N_s^{-1} \sum_{i,j} \|v_i - v_j\|^2$ , and the number of inactive control components. With  $N_s N_T = 3 \times 10^6$  control variables, Table I summarizes the results.

TABLE I

**TEST 2. CONTROL PERFORMANCE WITH  $\alpha = 0.01$ .**

Scenario	$V(T)$	Inactive controls
Uncontrolled	$2 \times 10^{-1}$	$3 \times 10^6$
Sparse ( $\beta = 10^{-1}$ )	$5 \times 10^{-4}$	$2 \times 10^6$
Full control	$9 \times 10^{-7}$	0

Sparse control greatly reduces dispersion with two-thirds of the components inactive, while full control achieves near-perfect alignment at full activation, illustrating the performance–sparsity trade-off.

### C. Test 2: Mean-field two dimensional dynamics

We now consider the two-dimensional mean-field CS system with final time  $T = 2$ , time step  $\Delta t = 0.05$ , and  $N = 10^4$  particles. The initial density  $f^0(x, v)$  consists of two symmetric clusters centered at  $(-5, 0)$  and  $(5, 0)$ , each uniformly distributed over a disc of radius  $r_{\max} = 2$ . Velocities depend quadratically on the distance from the origin, and include small Gaussian noise, producing two groups moving respectively along the directions  $(-1, 1)$  and  $(1, -1)$ . This yields a strongly misaligned configuration. The control problem is discretized as in (8)–(9), with quadratic penalization parameter  $\alpha = 0.01$ , sparsity  $\beta = 0.1$ , and global budget constraint  $\bar{B} = 10^6$ . The TOS algorithm is run with the same parameters used in the previous test. Figure 5 shows the two-dimensional mean-field test, reporting the spatial marginals at  $t = 0.8$  for  $\beta = 0$  (left) and  $\beta = 0.1$  (right). Without sparsity, the control induces stronger deformation, while for  $\beta = 0.1$  the action is more localized. Arrows show the momentum field, and the color intensity reflects the magnitude of the control. Figure 6 shows the

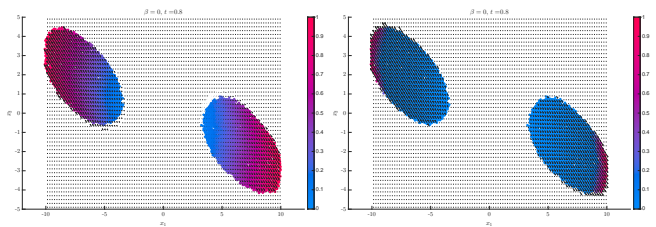


Fig. 5. **Test 3**. *Bottom row*: Spatial marginals at  $t = 0.8$  for  $\beta = 0$  (left) and  $\beta = 0.1$  (right). Arrows indicate the momentum field, the scale of color the magnitude of the control.

activation pattern of the control and the decay of  $V(t)$ . For  $\beta = 0$  the control stays fully active and  $V(t)$  decreases rapidly, whereas  $\beta = 10^{-1}$  yields sparser activation and a slower decay.

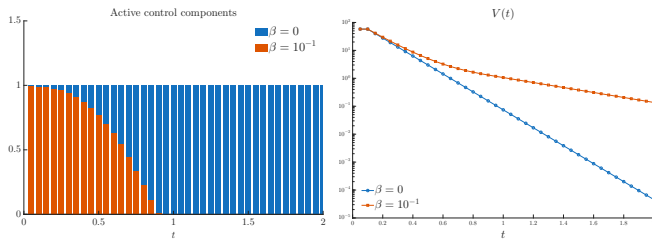


Fig. 6. **Test 2.** *Left:* Active control components over time for  $\beta = 0$  and  $\beta = 10^{-1}$ . *Right:* Decay of  $V(t)$  for the different  $\beta$  penalization regime.

## VI. CONCLUSION

This work presented an efficient framework for sparse stabilization of large-scale multi-agent systems, balancing control performance and computational cost. Using proximal methods, we obtained sparse controls that drive the system to consensus with reduced effort, while the mean-field formulation ensured scalability. The numerical results consistently confirm the effectiveness of the approach.

## REFERENCES

- [1] F. Cucker and S. Smale, "Emergent behavior in flocks," *IEEE Trans. Autom. Contr.*, vol. 52, no. 5, pp. 852–862, 2007.
- [2] M. R. D'Orsogna, Y.-L. Chuang, A. L. Bertozzi, and L. S. Chayes, "Self-propelled particles with soft-core interactions: patterns, stability, and collapse," *Phys. Rev. Lett.*, vol. 96, no. 10, p. 104302, 2006.
- [3] I. D. Couzin, J. Krause, N. R. Franks, and S. A. Levin, "Effective leadership and decision-making in animal groups on the move," *Nature*, vol. 433, pp. 513–516, 2005.
- [4] R. Hegselmann, U. Krause *et al.*, "Opinion dynamics and bounded confidence models, analysis, and simulation," *Journal of artificial societies and social simul.*, vol. 5, no. 3, 2002.
- [5] E. Cristiani, B. Piccoli, and A. Tosin, *Multiscale Modeling of Pedestrian Dynamics*, ser. Modeling, Simulation & Applications. Springer, 2014.
- [6] G. Albi, M. Bongini, E. Cristiani, and D. Kalise, "Invisible control of self-organizing agents leaving unknown environments," *SIAM J. Appl. Math.*, vol. 76, no. 4, pp. 1683–1710, 2016. [Online]. Available: <https://doi.org/10.1137/15M1017016>
- [7] G. Albi, F. Ferrarese, and C. Segala, *Optimized Leaders Strategies for Crowd Evacuation in Unknown Environments with Multiple Exits*. Cham: Springer International Publishing, 2021, pp. 97–131. [Online]. Available: [https://doi.org/10.1007/978-3-030-91646-6\\_5](https://doi.org/10.1007/978-3-030-91646-6_5)
- [8] H. Zhao, H. Liu, Y.-W. Leung, and X. Chu, "Self-adaptive collective motion of swarm robots," *IEEE Transactions on Automation Science and Engineering*, vol. 15, no. 4, pp. 1533–1545, 2018.
- [9] M. Duarte, V. Costa, J. Gomes, T. Rodrigues, F. Silva, S. M. Oliveira, and A. L. Christensen, "Evolution of collective behaviors for a real swarm of aquatic surface robots," *PLoS one*, vol. 11, no. 3, p. e0151834, 2016.
- [10] D. Ha and Y. Tang, "Collective intelligence for deep learning: A survey of recent developments," *Collective Intelligence*, vol. 1, no. 1, p. 26339137221114874, 2022.
- [11] J. A. Carrillo, M. Fornasier, G. Toscani, and F. Vecil, "Particle, kinetic, and hydrodynamic models of swarming," in *Mathematical modeling of collective behavior in socio-economic and life sciences*. Springer, 2010, pp. 297–336.
- [12] L. Pareschi and G. Toscani, *Interacting multi-agent systems. Kinetic equations & Monte Carlo methods*. USA: Oxford University Press, 2013.
- [13] G. C. Maffettone, M. Porfiri, and M. Di Bernardo, "Continuification control of large-scale multiagent systems under limited sensing and structural perturbations," *IEEE Control Systems Letters*, vol. 7, pp. 2425–2430, 2023.
- [14] G. Albi, M. Herty, and L. Pareschi, "Kinetic description of optimal control problems and applications to opinion consensus," *Commun. Math. Sci.*, vol. 13, no. 6, pp. 1407–1429, 2015. [Online]. Available: <https://doi.org/10.4310/CMS.2015.v13.n6.a3>
- [15] G. Albi and L. Pareschi, "Binary interaction algorithms for the simulation of flocking and swarming dynamics," *Multiscale Model. Simul.*, vol. 11, no. 1, pp. 1–29, 2013. [Online]. Available: <https://doi.org/10.1137/120868748>
- [16] S. Jin, L. Li, and J.-G. Liu, "Random Batch Methods (RBM) for interacting particle systems," *J. Comput. Phys.*, vol. 400, p. 108877, 2020.
- [17] G. Albi, S. Bicego, and D. Kalise, "Control of high-dimensional collective dynamics by deep neural feedback laws and kinetic modelling," *Journal of Computational Physics*, p. 114229, 2025.
- [18] M. Caponigro, M. Fornasier, B. Piccoli, and E. Trélat, "Sparse stabilization and optimal control of the Cucker-Smale model," *Math. Control Relat. Fields*, vol. 3, no. 4, pp. 447–466, 2013.
- [19] R. Bailo, M. Bongini, J. A. Carrillo, and D. Kalise, "Optimal consensus control of the Cucker-Smale model," *IFAC-PapersOnLine*, vol. 51, no. 13, pp. 1–6, 2018.
- [20] E. J. Candes, J. K. Romberg, and T. Tao, "Stable signal recovery from incomplete and inaccurate measurements," *Communications on Pure and Applied Mathematics: A Journal Issued by the Courant Institute of Mathematical Sciences*, vol. 59, no. 8, pp. 1207–1223, 2006.
- [21] D. L. Donoho, "Compressed sensing," *IEEE Transactions on information theory*, vol. 52, no. 4, pp. 1289–1306, 2006.
- [22] J. Cheng, B. Hofmann, M. Fornasier, H. Rauhut, J. Borwein, L. D. Russell, C. Byrne, P. Eggermont, M. Burger, B. Kaltenbacher *et al.*, "Handbook of mathematical methods in imaging: Volume 1," 2015.
- [23] M. A. Cohen and S. Grossberg, "Absolute stability of global pattern formation and parallel memory storage by competitive neural networks," *IEEE transactions on systems, man, and cybernetics*, no. 5, pp. 815–826, 1983.
- [24] M. Bongini and M. Fornasier, *Sparse Control of Multiagent Systems*. Cham: Springer International Publishing, 2017, pp. 173–228. [Online]. Available: [https://doi.org/10.1007/978-3-319-49996-3\\_5](https://doi.org/10.1007/978-3-319-49996-3_5)
- [25] M. Caponigro, M. Fornasier, B. Piccoli, and E. Trélat, "Sparse stabilization and control of alignment models," *Math. Models Methods Appl. Sci.*, vol. 25, no. 3, pp. 521–564, 2015. [Online]. Available: <https://doi.org/10.1142/S0218202515400059>
- [26] A. Beck, *First-Order Methods in Optimization*. Philadelphia, PA: Society for Industrial and Applied Mathematics, 2017. [Online]. Available: <https://epubs.siam.org/doi/abs/10.1137/1.9781611974997>
- [27] D. Davis and W. Yin, "A three-operator splitting scheme and its optimization applications," *Set-Valued and Variational Analysis*, vol. 25, 12 2017.
- [28] M. Fornasier, B. Piccoli, and F. Rossi, "Mean-field sparse optimal control," *Philos. Trans. R. Soc. Lond. Ser. A Math. Phys. Eng. Sci.*, vol. 372, no. 2028, pp. 20130400, 21, 2014. [Online]. Available: <https://doi.org/10.1098/rsta.2013.0400>
- [29] M. Fornasier and F. Solombrino, "Mean-field optimal control," *ESAIM Control Optim. Calc. Var.*, vol. 20, no. 4, pp. 1123–1152, 2014. [Online]. Available: <https://doi.org/10.1051/cocv/2014009>
- [30] D. Lacker, "Limit theory for controlled mckean-vlasov dynamics," *SIAM Journal on Control and Optimization*, vol. 55, no. 3, pp. 1641–1672, 2017.
- [31] G. Albi, Y.-P. Choi, M. Fornasier, and D. Kalise, "Mean field control hierarchy," *Applied Mathematics & Optimization*, vol. 76, no. 1, pp. 93–135, 2017.
- [32] M. Bongini and M. Fornasier, "Sparse stabilization of dynamical systems driven by attraction and avoidance forces," *Networks & Heterogeneous Media*, vol. 9, no. 1, p. 1, 2014.
- [33] D. Kalise, K. Kunisch, and Z. Rao, "Infinite horizon sparse optimal control," *Journal of Optimization Theory and Applications*, vol. 172, no. 2, pp. 481–517, 2017.
- [34] M. Fornasier, S. Lisini, C. Orrieri, and G. Savaré, "Mean-field optimal control as gamma-limit of finite agent controls," *European J. Appl. Math.*, vol. 30, no. 6, pp. 1153–1186, 2019.
- [35] M. Herty and C. Ringhofer, "Consistent mean field optimality conditions for interacting agent systems," *Communications in Mathematical Sciences*, vol. 17, no. 4, pp. 1095–1108, 2019.
- [36] M. Burger, R. Pinnau, C. Totzeck, and O. Tse, "Mean-field optimal control and optimality conditions in the space of probability measures," *SIAM Journal on Control and Optimization*, vol. 59, no. 2, pp. 977–1006, 2021.